Actas de las XXXIX Jornadas de Automática, Badajoz, 5-7 de Septiembre de 2018
https://doi.org/10.17979/spudc.9788497497565.0748

STUDY IN COMSOL OF THE GENERATION OF TRAVELING WAVES IN AN AEF ROBOT BY PIEZOELECTRIC ACTUATION

Javier Prieto-Arranz[1], José Emilio Traver[2], Miguel A. López[2], Inés Tejado[2], Blas M. Vinagre[2]
[1]School of Industrial Engineering, University of Castilla-La Mancha, 13071 Ciudad Real, Spain.
email: Javier.PrietoArranz@uclm.es
[2]Industrial Engineering School, University of Extremadura, 06006 Badajoz, Spain.
email: milopezr@alumnos.unex.es, {jetraverb;itejbal;bvinagre}@unex.es

Abstract

This paper presents a study of motion of an artificial eukaryotic flagellum (AEF) microrobot in COMSOL Multiphysics®. The microrobot is essentially a body, consisting of an aluminum beam structure with two piezoelectric patches bonded on its surface. It requires the same voltage with different frequencies or phases be applied to each piezoelectric or use one of the piezoelectrics as absorber in order to generate a traveling wave on the body. Different types of actuation are simulated to demonstrate that a non-reciprocal motion can be obtained with this kind of configuration.

Keywords: Robot, Eukaryotic, Beam, Piezoelectric, Planar Wave, Traveling wave, Simulation, COMSOL

1 INTRODUCTION

The field of submillimeter scale robots (micro and nanorobots) is receiving much attention recently as a result of the advances in technology. Some examples that can be found in the literature are microrobots that can access small spaces down to the micro scale, such as inside the human body by making existing therapeutic and diagnostic procedures less invasive [7, 14], and robots that manipulate and interact with tiny entities of the environment for inspection tasks in infrastructures [19, 25] or machines [1], and for search and rescue in natural catastrophes [9, 23]. Refer to e.g. [2, 15, 18] for more examples of applications.

However, working at micro and nanoscale involves a great number of challenges, beginning from fabrication techniques, control, ways to supply power, and propulsion. The principles governing the design of such scale robots rely on the understanding of microscale physics and dynamics. To this respect, the Reynolds number (Re), a relation between inertial and viscous forces according to environment, is another key point to take into account for microrobots design. Our current research interests are inspired by emulating locomotion of biological swimmers, more specifically of eukaryotic cells.

In the literature several ways of generating non-reciprocal motion in low Re environment have been analyzed. The main kinds are based on the helical motion of a bacterial flagellum implemented with magnetic actuation and internal motor [17, 14], and those based on the generation of planar waves by means of an eukaryotic flagellum (traveling wave). This last kind can be approached with several methods: 1) by distributed actuation [12, 20, 21, 22], 2) by actuation in two-point [5, 6], and 3) by single-point actuation with reflected wave absorption [5, 6] or single-point actuation with non-uniform mass distribution [11]. Notice that some of these methods have been investigated in our previous works.

In this context, this paper studies the generation of a traveling wave in a beam-based artificial eukaryotic flagellum (referred to as BAEF) using piezoelectric patches bonded on its surface and testing different kinds of actuation. This work is based on two ideas: 1) the motion of ultrasonic motors [24], which generate a linear traveling wave in a finite beam by means of two-point excitation (referred to as 2PE), and 2) the reduction of structural vibrations by shunting an attached piezoelectric transducer with an electrical impedance [4, 13], where only one-point excitation is needed (1PE). Simulations in COMSOL Multiphysics are given to demonstrate that the designed beam-based robot is able to produce a non-reciprocal motion for propulsion. As will be shown, the design of the flagellum consists of an aluminum beam with two piezoelectric patches bonded on its surface close to its ends.

The remainder of the paper is organized as follows. Motion in a low Re number environment is summarized in Section 2. Section 3 describes operation principles of the generation of traveling waves. Section 4 gives the details of the robot model developed in COMSOL® and explains how the beam is deformed. Results are discussed in Section 5. Finally, conclusions and future works

are drawn in Section 6.

2 MOTION IN A LOW REYNOLDS NUMBER ENVIRONMENT

This section presents the characteristics of fluid environments and other considerations needed to understand the effects of microscopic scale at macroscopic level. It also describes the kinds of motions that allow swimming in such environments.

2.1 HYDRODYNAMICS

The hydrodynamics of macroscopic swimming robots is governed by the Navier-Stokes equation, which is defined for an incompressible fluid by:

$$\frac{\partial V}{\partial t} + (V \cdot \nabla)V - \frac{\mu}{\rho}\nabla^2 V = -\frac{1}{\rho}\nabla P + F \quad (1)$$

where t is time, ρ and μ are fluid's density and dynamic viscosity, respectively, V is the velocity vector, P is pressure, and F represents other external forces. This equation is only suitable for regimes with high Re, that means that the inertial terms (the two first terms on the left of (1)) are far higher than viscous terms. This indicates that such robots, within environments with high Re are based on inertia to swim.

However, the viscous forces predominate over inertial at small scale (from milli to micrometers), which results in a low Re and, thus, swimming robots experiment a different hydrodynamics. For this regime, (1) reduces to Stokes' equation:

$$-\frac{\mu}{\rho}\nabla^2 V + \frac{1}{\rho}\nabla P = F \quad (2)$$

The hydrodynamics defined by Stokes' equation indicates that the change of velocities does not produce a propulsion motion; this is the case of scallop, because the produced inertial forces are negligible. Therefore, a non-reciprocal and irreversible in time motion is need to swim [16, 14]. To obtain at macroscopic scale the same behaviour with low Re, all involved variables have to be scaled through this dimensionless parameter. Taking into account that Re can be mathematically expressed as:

$$Re = \frac{\rho V L}{\mu}, \quad (3)$$

setting the size of the robot (L), a fluid with the proper ρ/μ relation must be used for the expected forward speed (V).

2.2 PROPULSION WAVEFORMS

The propulsion waveform in an environment with low Re achieves a great importance. As explained above, only a non-reciprocal motion allows the propulsion in that environment. Different kinds of propulsion waveforms are observed in biological swimmers. The first kind is a planar (traveling) wave based on flagella of eukaryotic cells. It was studied by Gray and Hancock in [3] and described as a traveling harmonic wave. The second and third waveforms define the Carangiform fishes motion (the bending of their bodies in a propulsive wave that extends from head to tail end). This motion was described using a traveling wave function by Lighthill [10].

These three waveforms can be described by the following expression:

$$y(x,t) = (c_0 + c_1 x + c_2 x^2)\sin\left(\frac{2\pi}{\lambda}(x - V_p t)\right), \quad (4)$$

where c_0, c_1 and c_2 are the coefficients that govern the amplitude growing, x is the displacement along the propulsion axis, V_p refers to the propagation speed of the wave, and λ is the wavelength. For planar waves, the amplitude is only given by coefficient c_0 (the others are zero). For Carangiform swimmers, $c_0 = 0$. By choosing adequate values for c_1 and c_2 coefficients, two important properties for propulsion can be preserved: 1) the flagellum head is always maintained at zero amplitude (boundary condition, i.e., $y(0,t) = 0$), and 2) the wave amplitude along the flagellum can be modulated.

An alternative way for preserving such properties is the use of a fractional power of growing for variable x as follows [20]

$$y(x,t) = (cx^{\alpha})\sin\left(\frac{2\pi}{\lambda}(x - V_p t)\right), \quad (5)$$

where c defines the amplitude at end of flagellum

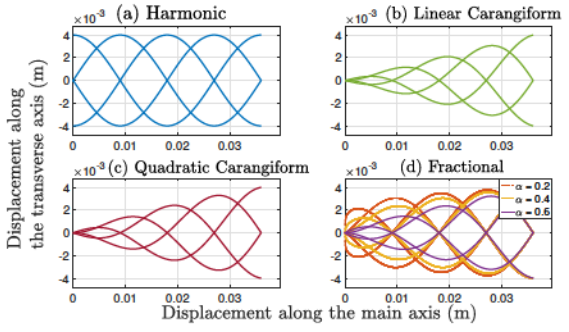

Figure 1: Appearance of the four different kinds of traveling waves: (a) Harmonic (b) Linear Carangiform (c) Quadratic Carangiform (d) Fractional

and $\alpha \in \mathbb{R}^+$ $(0 < \alpha < 1)$ is the fractional order coefficient of the wave, whose value determines the way of growing. In particular, when $\alpha = 0$, the resulting waveform is harmonic, whereas when $\alpha = 1$, it results in the Carangiform swimmer waveform. Thus, this waveform can be also viewed as a generalization of the previous waves, merging the features from planar to Carangiform swimming wave. Figure 1 depicts the four traveling waveforms described.

3 OPERATION PRINCIPLES OF GENERATION TRAVELING WAVE

Traveling wave are rarely observed on finite structures owing to the reflect of vibration waves when it hits the boundaries, which creates the superposition of two traveling waves in opposite direction resulting in a standing wave. Standing waves are the general vibration case on finite structured, but traveling waves can be generated under certain conditions: 1) by standing waves generates with two-point excitation [24, 6], or 2) by removing the reflected waves using a shunting piezoelectric with an electrical impedance to dissipate the mechanical energy converted in electrical energy previously [13, 5]. Next, the former operation principle to generate a traveling wave on finite structure beam is described.

3.1 TWO-POINT EXCITATION

As mentioned, the standing wave is a case of two-wave interference. Therefore, a traveling wave can be generated as the result of the summation of two standing waves that are excited according to certain conditions. The mechanical displacement of the beam between actuator must have a spatial difference and temporal phase of 90° and the excitation frequency must be between two vibration modes [24]. Let assume that the voltage applied in each piezoelectric is $V_{PZ1} = \cos(\omega t)$ and $V_{PZ2} = \cos(\omega t + \alpha)$, being ω the excitation frequency and α is the temporary phase. In accordance with [24], the phase needed to achieve the former conditions have to be $\alpha = \pi(n-m)/2$ with $m = \pm 2K + 1$ and $n = \pm 2K$ with $K \in \Re$ and the wavelength of traveling wave created is defined as $\lambda = 4d/(n+m)$, where d is the distance between piezoelectrics. A scheme of the 2ME is illustrated in Figure 2a.

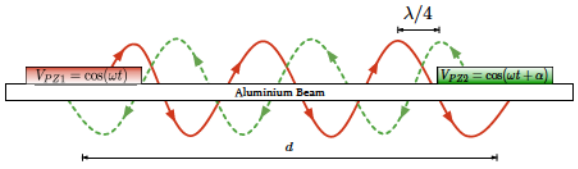

(a) Two-point excitation

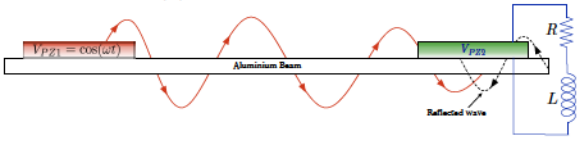

(b) One-point excitation

Figure 2: Scheme of excitation of the BAEF robot

3.2 ONE-POINT EXCITATION

In two-point excitation, two actuators are used as vibrators. The first produces a vibration on the beam whose reflected waves are compensated by the second with other vibration with different spatial and temporal phase. The generation of traveling waves with only one-point excitation is based on the reduction of the reflected wave at end of beam. According to shunt damping methodologies, one actuator is used as vibrator and other as a sensor to convert this mechanical vibration into heating by means of an electrical circuit [13, 5, 4].

The main approaches of shunt damping methodologies are often divided into: single-mode and multi-mode. This work only focuses on the first. Although they are simple and damp only one structural mode, they are enough to reduce the vibration and generate a traveling wave. Hagood and Von Flotow [4] developed a general shunted model for two shunt circuits: a resistor circuit alone and resistor–inductor (RL) circuits connected in series. For resistive shunting, they demonstrated that material properties exhibit frequency dependence similar to viscoelastic material. That frequency dependence is minimized with the second circuit, which allows to create an electrical resonance by shunting the inherent capacitance of the piezoelectric, and whose behaviour is analogous to that of a mechanical vibration absorber (see Figure 3). Other shunt circuits combine resistor and capacitor, but, in addition to demonstrate poorly performing, also involves a modification of effective stiffness of piezoelectric transducer [13].

The parameters of the RL shunt circuit have to be tuned to one structural node, similar to that of a

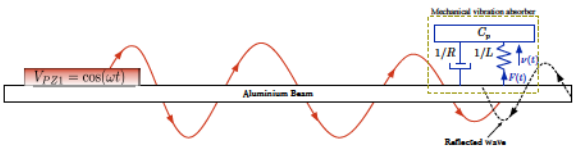

Figure 3: Mechanical equivalent model of shunt circuit (mass damper)

mechanical vibration absorber and thereby greatly increased the attainable modal damping ratio, in an effect similar to resonant vibration absorber [4]. Hagood and Von Flotow calculated a relation to tune the series shunt circuit according to vibration mode to be damped:

$$R = \frac{\sqrt{2}K_{31}}{C_p \omega_n^D (1 + K_{31}^2)} \tag{6}$$

and

$$L = \frac{1}{(\omega_n^E)^2 C_p^S} \tag{7}$$

where K_{31} is the electromechanical coupling factor defined as

$$K_{31} = \sqrt{\frac{(\omega_n^D)^2 - (\omega_n^E)^2}{(\omega_n^E)^2}},$$

and w_n^D is the resonance frequency to be damped when the shunt circuit is open, w_n^D is the same resonance frequency when the circuit is shorted, and C_p^S is the inherent capacitance of the piezoelectric measured at constant strain, which can be calculated as:

$$C_p^S = C_p^T (1 + k_{31}^2),$$

being C_p the capacitance of the piezoelectric measured at constant mechanical stress and k_{31} is a electromechanical coupling factor provided by the manufacturer.

4 MODELING IN COMSOL MULTIPHYSICS

This section gives the details of the model of the beam robot developed in COMSOL Multiphysics and explains how to emulate the propulsion waveforms of eukaryotic cells.

4.1 GEOMETRY OF THE MODEL

The beam artificial eukaryotic flagella robot is designed and simulated in COMSOL through a 2D model. Its design is again inspired by biological swimmers, specifically by a sperm cell. It consists of an beam with two piezoelectric patches bonded on its surface and close to its ends, as shown in Figure 4.

The material chosen for piezoelectrics is APC-851 (Navy Type II), whose properties are similar to the material that was concluded in our previous work [12] as the more adequate to generate a traveling wave with distributed actuation. In order to be able to consider a model in 2D, the length of

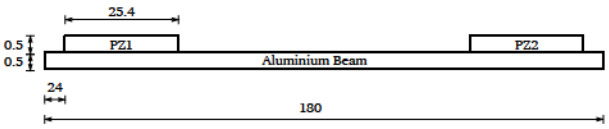

Figure 4: Model of beam-based artificial eukaryotic flagella robot (units are given in mm)

each piezoelectric is chosen as twice its width, allowing to consider only the dynamics corresponding to the direction parallel its length. Likewise, the selection of its thickness is based on the study in [6], where it was stated that the larger the thickness of the piezoelectric, the more important the bending stiffness of the system in comparison with the bending moment generated by the piezoelectric. For that reason and with the second purpose to reduce power to excite them, low thickness is desired. In what the material is concerned, it is used aluminum because it has better elastic behaviour than other materials for this application [6]. Consequently, the width and thickness of robot body is equal to those of the piezoelectrics, whereas its length is three times the sum of that of both piezoelectrics, to be able to generate a traveling wave with different wavelengths. The properties and dimension of aluminum beam (body) and piezoelectrics are given in Table 1.

The positions of the piezoelectrics have a great influence on the traveling wave performance [5]. For example, when the piezoelectrics are placed near to the middle of beam, the vibrations are less progressive, and the wavelength and number of waves are also less, with what the performance of propulsion wave would be reduced. For this reason, the piezoelectrics are located close to the tips of the beam, concretly at $x_{pz1} = 24$ mm and $x_{pz2} = 130.6$ mm.

4.2 PHYSICS INTERFACES

The set of physics selected for this application are:

- *Solid mechanics*, which allows to study the stress and elastic deformation that the beam is subjected to when a force is applied over it. It is worth to mention that, for the model

Table 1: Body (beam) and piezoelectric properties

	Aluminum	PZT - APC 851
Length × Width × Thickness (mm)	25.4 × 12.7 × 0.5	25.4 × 12.7 × 0.5
Young's modulus (Pa)	69×10^9	-
Poison's ratio	0.33	-
Volume density (kg·m^{-3})	2700	7900
Relative permittivity [ε_{33r}]	-	1900
Piezoelectric constant [d_{31}] (mV^{-1})	-	-175×10^{-12}
Elastic compliances [s_{11}] (Pa^{-1})	-	1.58×10^{-11}
[s_{12}] (Pa^{-1})	-	-1.85×10^{-11}
Electromechanical Coupling Factor [k_{31}]	.	0.36

to behave as future experimental setup, correct damping coefficients need to be applied. Due to the dynamic nature, and frequency dependent damping, Rayleigh damping is used. Because no experimental data is available, damping ratio for aluminum can be approximated as equal to 0.02% [8].

- *Electrostatic*, which considers the electrical dynamics of the piezoelectrics when a voltage is applied between their surfaces.
- *Electrical circuit*, which, together with the *electrostatic* physics, allow to model and include the dynamics of the excitation circuit (2PE) and shunt circuits (1PE), considering the power consumption and dissipation through the Joule effect.
- Multiphysics *piezoelectric effect*, which is in charge of interpreting the mechanical and electrical coupling present in the piezoelectric materials.

Thus, a complete system is built coupling all physics, where a mechanical change has an effect on electrical dynamics and vice versa. The discretization of model is realized with a mesh of the free triangular kind. The elements size is set to 72 μm and 360 μm for the minimum and maximum size, respectively. With this configuration, it is defined a system with 16242 degrees of freedom.

5 RESULTS

This section presents the results obtained when simulating the beam robot in the following scenarios: 1) mode of vibrations of beam and the influence of the piezoelectrics on the dynamics of the beam, 2) the generation of a traveling and standing wave with two-point excitation, and 3) the generation traveling wave with one-point excitation. Furthermore, they will be compared with the corresponding of the ideal motion.

With the purpose to validate the results in futures works, all studies are realized with the beam robot clamped and a maximum voltage of excitation for piezoelectrics of 20 V.

5.1 MODES OF VIBRATION

The firs step is to know the modes of vibrations of beam and how they are affected by the addition of piezoelectric material. In Table 2 is shown the theoretical modes of vibration of beam, the obtained from FEM model in COMSOL and with the addition of piezoelectric. The results of simulations are agree with theoretical data, although the results drift slightly for high frequencies.

Table 2: Vibrations modes

Mode	Theoretical (Hz)	FEM Beam (Hz)	FEM Beam + PZT (Hz)
1	12.44	13.45	11.48
2	77.97	84.39	81.41
3	218.32	236.31	215.11
4	427.82	463.02	461.34
5	707.23	765.32	867.4
7	1475.6	1596.3	1844.9
8	1964.5	2124.8	2305
14	6365.1	6872.1	6338
15	7343	7503.2	7783.4

When attaching the piezoelectrics, Figure 5, where the frequency response of beam is depicted when an force is applied in the free end. As can be seen, the dynamics on the beam is slightly affected, as shown in . In addition, Figure 5 also includes the frequency response of beam robot when the first piezoelectric is excited and the second is shorted. From this last result, it must be remarked its dynamics is similar to the others with the exception that antiresonance are removed as result of the shorted of the second piezoelectric.

5.2 TWO-POINT EXCITATION

When two-point excitation is used to generate a traveling wave, according to explained in the section 3.1 a difference of phase between excitations are required. However, this requirement is necessary, but not sufficient. If the excitation frequency is equal to one resonance frequency, the reflected wave is not cancelled and standing wave is created, and thus a reciprocal motion, as shown in the Figure 6. The right figure shows a ideal standing wave whose antinodes swept alternately between the maximum and minimum deformation, and the left figure shows the simulation results with a similar behaviour.

Therefore, a properly excitation frequency must be chosen between two resonance frequencies. Allowing to cancel the reflected wave and generate a traveling wave. The results obtained from simulation for a frequency excitation between 14^{th} and 15^{th} resonance frequency are shown in the

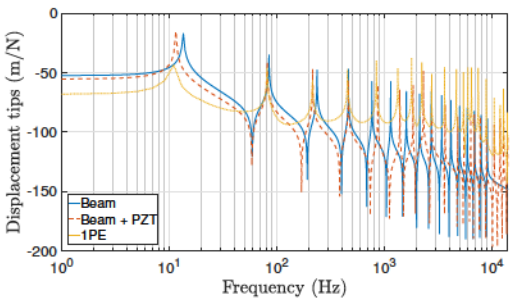

Figure 5: Frequency response of the model for different configurations

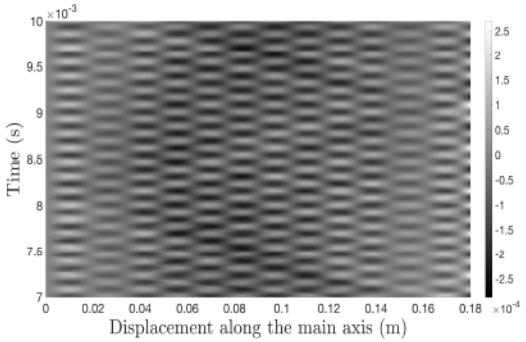

(a) Displacement results of the simulation.

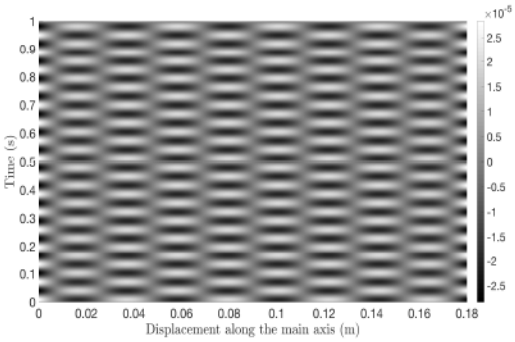

(b) Ideal displacement of traveling wave.

Figure 6: Time response of two-point excitation at 14^{th} resonance frequency

Figure 7. The Figure 7b depicts the ideal case where the wave propagates along the beam, and thus there is not nodes and anti-nodes, and the Figure 7a shows displacement for the new excitation frequency, that corresponds with a progressive wave.

5.3 ONE-POINT EXCITATION (1ME-RL)

The results for one point excitation are shown in the Figure 8, where it can be seen how a traveling wave is generated tuning the shunt circuit parameters with the relations indicate in (6) and (7). In contrast to two point excitation, with this method the piezoelectric can excited at one frequency of resonance to generate the traveling wave. It is also worth to mention that traveling wave is only generated between two piezoelectric, the rest of beam shows a stationary behaviour. Thus the number of waves or wavelength is limited by this distance, and consequently, the propulsion performance. By the other hand, these parameter are also related with excitation frequency and propulsion speed,

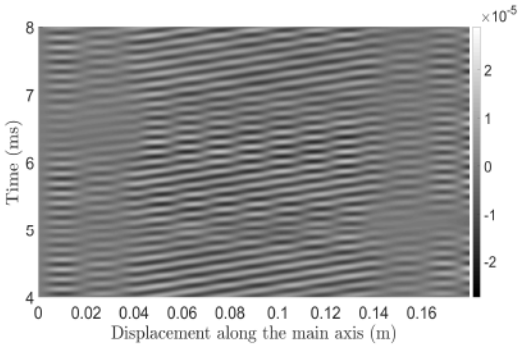

(a) Displacement results of the simulation.

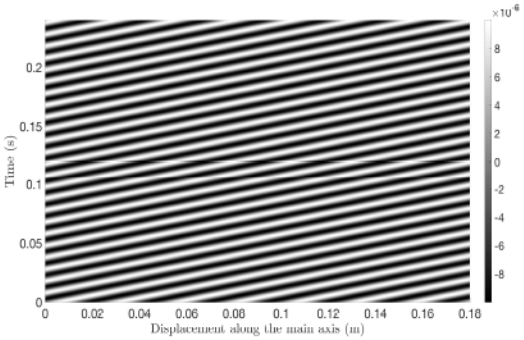

(b) Ideal displacement of traveling wave.

Figure 7: Time response of two-point excitation between 14^{th} and 15^{th} resonance frequency.

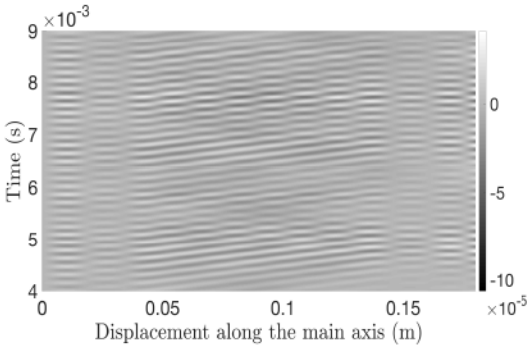

(a) Displacement for an excitation frequency at the 14^{th} resonance frequency.

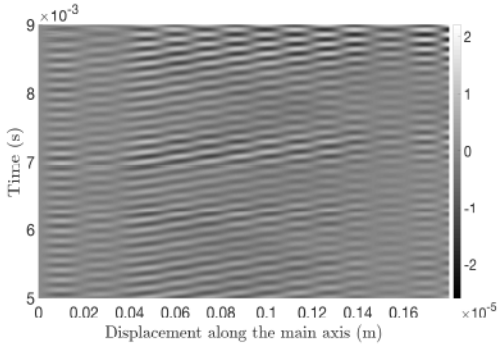

(b) Displacement for an excitation frequency between 14^{th} and 15^{th} resonance frequency.

Figure 8: Time response of one-point excitation with RL shunt circuit.

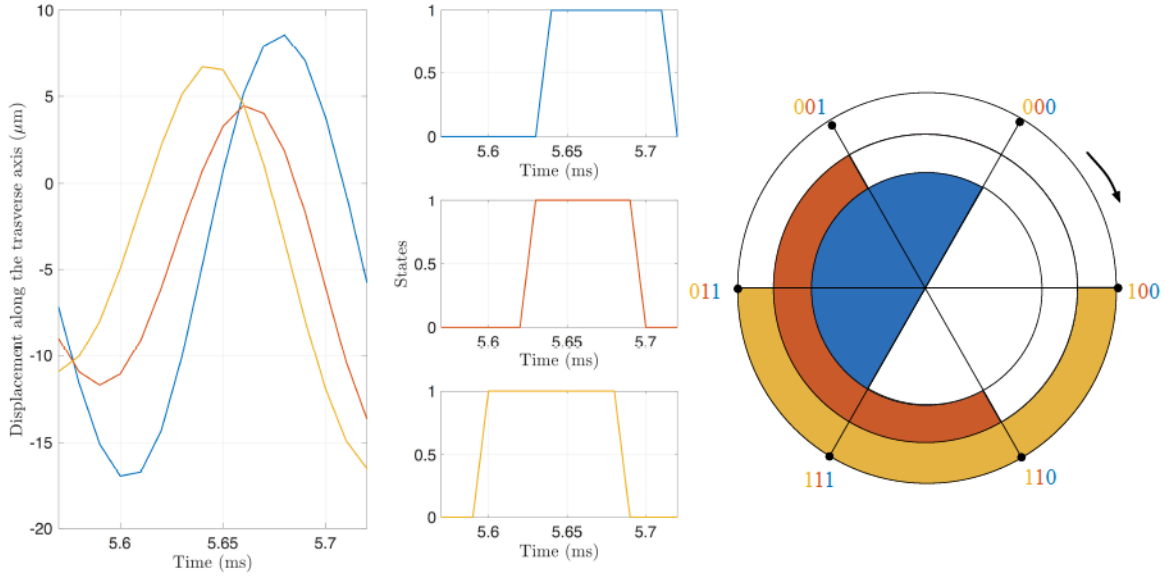

Figure 9: Displacement of beam robot with one-point excitation at the 14^{th} resonance frequency and its coding.

allowing to control this last through the excitation frequency.

One of the key aspects to be taken into account for the flagellum motion is, as mentioned above, its non-reciprocity [16]. Figure 9 shows the motion obtained codified (on the right in this figure), as 1 if the displacement is higher of mean and 0 whereas it is lower or equal. As can be observed, the flagellum motion is non-reciprocal. Likewise, it proves that excitation method is enough to make the desired motion with piezoelectric actuators.

6 CONCLUSIONS

This paper has studied the motion of an artificial eukaryotic flagellum robot in COMSOL Multiphysics. A 2D model of beam robot has been simulated in COMSOL and time dependent and frequency studies were done with the objective to create a traveling wave on limited structure.

The simulation results showed that methodologies presented can be used to create a traveling wave with one or two point excitation. In addition, they determine that a single excitation is enough to allow propulsion in low *Re* environments and the excitation frequency could control the propulsion speed.

Our future works will go towards two directions: 1) the fabrication of robot and its test in different scenarios, and 2) the implementation of an adaptive frequency shunt circuit and study of dynamic in a low *Re* environment

Acknowledgment

This work has been supported by the Spanish Ministry of Economy and Competitiveness under the project with reference DPI2016-80547-R.

References

[1] Nikolaus Correll and Alcherio Martinoli. Multirobot inspection of industrial machinery. *IEEE Robotics & Automation Magazine*, 16(1):103–112, 2009.

[2] Eric Diller and Metin Sitti. Micro-scale mobile robotics. *Foundations and Trends in Robotics*, 2(3):143–259, 2013.

[3] J. Gray and G. J. Hancock. The propulsion of sea-urchin spermatozoa. *Journal of Experimental Biology*, 32(4):802–814, 1955.

[4] Nesbitt W Hagood and Andreas von Flotow. Damping of structural vibrations with piezoelectric materials and passive electrical networks. *Journal of Sound and Vibration*, 146(2):243–268, 1991.

[5] Hassan Hariri, Yves Bernard, and Adel Razek. A traveling wave piezoelectric beam robot. *Smart Materials and Structures*, 23(2):025013, 2013.

[6] Hassan Hariri, Yves Bernard, and Adel Razek. Dual piezoelectric beam robot: The effect of piezoelectric patches' positions. *Journal of Intelligent Material Systems and Structures*, 26(18):2577–2590, 2015.

[7] Ian W Hunter, Tilemachos D Doukoglou, Serge R Lafontaine, Paul G Charette, Lynette A Jones, Mark A Sagar, Gordon D Mallinson, and Peter J Hunter. A teleoperated microsurgical robot and associated virtual environment for eye surgery. *Presence: Teleoperators & Virtual Environments*, 2(4):265–280, 1993.

[8] Robert Jansson. Simulation and study of passive shunt damping of a composite plate by embedded pzt transducers, 2016.

[9] Vijay Kumar, Daniela Rus, and Sanjiv Singh. Robot and sensor networks for first responders. *IEEE Pervasive Computing*, 3(4):24–33, 2004.

[10] MJ Lighthill. Note on the swimming of slender fish. *Journal of Fluid Mechanics*, 9(2):305–317, 1960.

[11] Miguel A. López, Javier Prieto, José Emilio Traver, Inés Tejado, Blas M. Vinagre, and Ivo Petrás. Testing non reciprocal motion of a swimmingflexible small robot with single actuation. *19th International Carpathian Control Conference*, 2018.

[12] Enrique Mancha, José Emilio Traver, Inés Tejado, Javier Prieto, Blas M Vinagre, and Vicente Feliu. Artificial flagellum microrobot. design and simulation in comsol. In *Iberian Robotics conference*, pages 491–501. Springer, 2017.

[13] SO Reza Moheimani and Andrew J Fleming. *Piezoelectric transducers for vibration control and damping*. Springer Science & Business Media, 2006.

[14] Bradley J Nelson, Ioannis K Kaliakatsos, and Jake J Abbott. Microrobots for minimally invasive medicine. *Annual Review of Biomedical Engineering*, 12:55–85, 2010.

[15] Igor Paprotny and Sarah Bergbreiter. *Small-Scale Robotics. From Nano-to-Millimeter-Sized Robotic Systems and Applications*, volume 8336 of *Lecture Notes in Computer Science*, chapter Small-Scale Robotics: An Introduction, pages 1–15. Springer-Verlag Berlin Heidelberg, 2014.

[16] Edward M Purcell. Life at low Reynolds number. *American Journal of Physics*, 45(1):3–11, 1977.

[17] Javier Silva, Javier Prieto, Inés Tejado, Emiliano Pérez, and Blas M. Vinagre. Robots nadadores tipo flagelo bacteriano de pequeñas dimensiones: Desarrollo de prototipos y plataformas de prueba. *XXXVII Jornadas de Automática*, 2016.

[18] Metin Sitti. Microscale and nanoscale robotics systems: Characteristics, state of the art, and grand challenges. *IEEE Robotics & Automation Magazine*, 14(1):53–60, 2007.

[19] D. A. Stepanenko, V. T. Minchenya, R. M. Asimov, and K. Zimmermann. Possibility of application of small-size robots with vibratory piezoelectric actuators for inspection of physical state of surfaces. In *Proceedings of the 2011 International Congress on Ultrasonics - Gdansk*, pages 685–688, 2011.

[20] José Emilio Traver, Inés Tejado, and Blas M Vinagre. New waveforms for propulsion of planar cial bacterial flagella microrobots. *In: Proceedings of VI Spanish Chapter of the European Society of Biomechanics*, 2016.

[21] José Emilio Traver, Inés Tejado, and Blas M Vinagre. A comparative study of planar waveforms for propulsion of a joined artificial bacterial flagella swimming robot. *Proceedings of 4th International Conference on Control, Decision and Information Technologies (CoDIT'17)*, 2017.

[22] José Emilio Traver, Blas M. Vinagre, and Inés Tejado. Robot nadador tipo flagelo bacteriano plano: estudio y simulación del mecanismo de propulsión. *XXXVII Jornadas de Automática*, pages 1075–1082, 2016.

[23] R. M. Voyles and A. C. Larson. TerminatorBot: a novel robot with dual-use mechanism for locomotion and manipulation. *IEEE/ASME Transactions on Mechatronics*, 10(1):17–25, 2005.

[24] Chunsheng Zhao. *Ultrasonic motors: technologies and applications*. Springer Science & Business Media, 2011.

[25] Raziq Asyraf Zin, Khairul Salleh Mohamed Sahari, Juniza Md Saad, Adzly Anuar, and Abd Talip Zulkarnain. Development of a low cost small sized in-pipe robot. *Procedia Engineering*, 41:1469–1475, 2012.